Accepted Manuscript

Primary vs. secondary curved fold axes: Deciphering the origin of the Aït Attab syncline (Moroccan High Atlas) using paleomagnetic data

B. Moussaid , J.J. Villalaín , A. Casas-Sainz , H. El Ouardi , B. Oliva-Urcia , R. Soto , T. Román-Berdiel , S. Torres-López

PII: S0191-8141(14)00264-8

DOI: 10.1016/j.jsg.2014.11.004

Reference: SG 3159

To appear in: *Journal of Structural Geology*

Received Date: 30 April 2014

Revised Date: 3 November 2014

Accepted Date: 9 November 2014

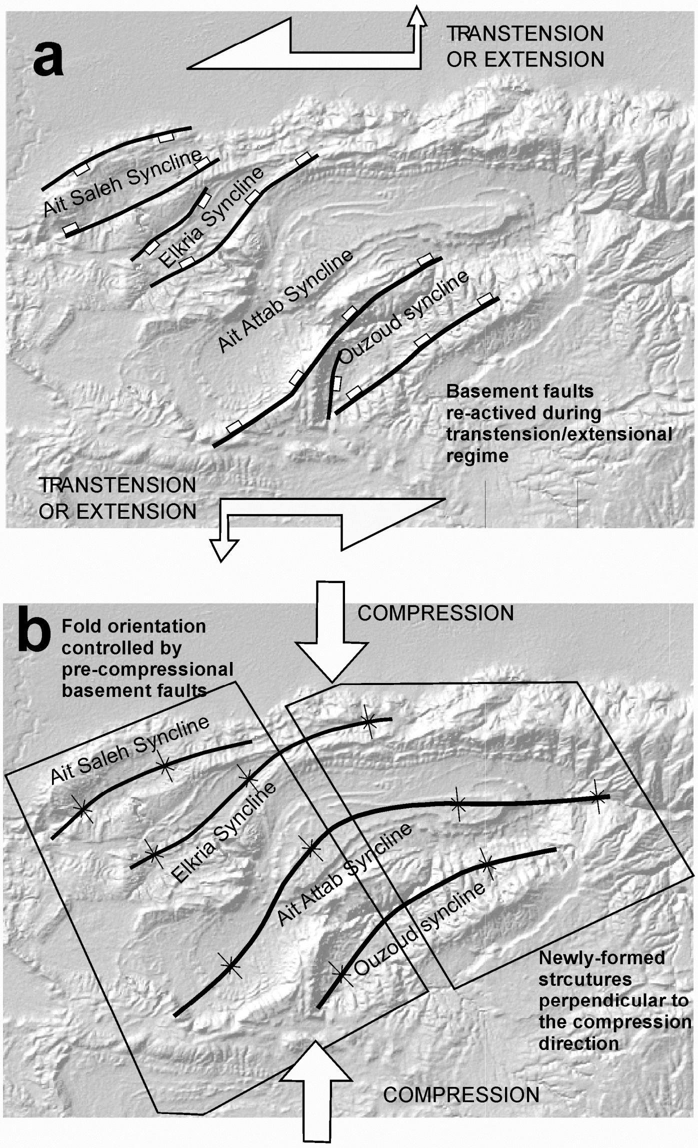
a
TRANSTENSION
OR EXTENSION
Ait Saleh Syncline
Elkria Syncline
Ait Attab Syncline
Ouzoud syncline
Basement faults
re-actived during
transtension/extensional
regime
TRANSTENSION
OR EXTENSION
b
COMPRESSION
Fold orientation
controlled by
pre-compressional
basement faults
Ait Saleh Syncline
Elkria Syncline
Ait Attab Syncline
Ouzoud syncline
Newly-formed
strcutures
perpendicular to
the compression
direction
COMPRESSION

Primary vs. secondary curved fold axes: deciphering the origin of the Aït Attab syncline (Moroccan High Atlas) using paleomagnetic data

B. Moussaid [1] , J.J.Villalaín[2], A.Casas-Sainz[3], H.El Ouardi[1], B.Oliva-Urcia[4], R. Soto[5], T. Román-Berdiel[3], and S. Torres-López[2]

(1) Dép. de Géologie, Faculté des Sciences, université Moulay Ismail, BP. 11201 Zitoune, Meknès, Maroc. bnmous@hotmail.fr ; hmidouelouardi@yahoo.fr

(2) Dpto. de Física. Escuela Politécnica Superior. Universidad de Burgos. Avd Cantabria S/N, 09006 Burgos, Spain. villa@ubu.es

(3) Dpto. de Ciencias de la Tierra, Facultad de Ciencias, Universidad de Zaragoza, 50009 Zaragoza, Spain. acasas@unizar.es

(4) Dpto.de Geologia y Geoquimica, Facutad de Ciencias. Universidad Autónoma de Madrid. Calle Francisco Tomás y Valiente, 7. Ciudad Universitaria de Cantoblanco. 28049 Madrid, Spain. Belen.oliva@uam.es

(5) Instituto Geológico y Minero de España, Unidad de Zaragoza, C/ Manuel Lasala 44, 9B, 50006 Zaragoza, Spain. r.soto@igme.es

Abstract

The Aït Attab syncline, located in the Central High Atlas, displays a curved geometry in plan view, and is considered as one of the most spectacular fold shapes in the Central High Atlasic belt. We conducted a paleomagnetic study in Jurassic-Cretaceous red beds to investigate the origin of this geometry. The Natural Remanent Magnetization (NRM) is dominated by a secondary magnetization carried by haematite with unvarying normal polarity that has been dated at about 100 Ma. The regional fold test performed in both limbs of the syncline is positive and the paleomagnetic vectors (after tectonic correction) are parallel throughout the curvature, indicating a negative oroclinal bending test. These results are inconsistent with previous works that consider the bent geometry of this syncline to result from subsequent distortion of originally NE-SW trending structures by rotation about a vertical axis. We interpret the NRM data to demonstrate that the changing trend of the Aït Attab syncline is a primary feature, resulting from the influence of pre-existing, NE-SW and E-W-striking extensional faults that developed during a strike-slip regime. Paleomagnetic results also reveal that the tilting observed in the sampled red beds is post Albian, probably linked to the Cenozoic inversion of the High Atlasic belt.

Key-words: Paleomagnetism, remagnetization, fold test, oroclinal bending, Aït Attab syncline, Moroccan High Atlas

1. Introduction

Curvatures in plan view in orogens, fold-and-thrust belts and single structures have been classified as primary, progressive or secondary orocline, based on their kinematics (e.g. Weil and Sussman, 2004). Unravelling which behavior applies to a particular structural setting is crucial to characterizing its deformational and kinematic history.

The Aït Attab syncline, located in the northern border of the High Atlasic belt in Morocco, shows a spectacular curved shape in plan view (fig. 1). Its axis is oriented E-W and NE-SW at its eastern and western segment, respectively. The Aït Attab syncline is defined by a Jurassic-Cretaceous sequence deposited in the Attab basin. The origin of its curved geometry can be attributed to several mechanisms: (i) superposed folding related to an accommodation zone (Beauchamp, 2004), (ii) oroclinal bending producing secondary curvature of structures and a sharp bend geometry, as demonstrated in several works for other curved belts (e.g. Schwartz and Van der Voo, 1983; Kent, 1988; Marshak, 1988), (iii) distortion of original folding structures linked to the influence of basement fault on the cover sediment (Ibouh, 2004), or (iv) geometry conditioned by the sigmoid shape of the sedimentary basin inherited from the extensional/transtensional origin. This basin geometry is linked to a strike-slip tectonic model as proposed by Laville (1985) for the Jurassic basin.

The present work aims to study the origin of the curved shape of the Aït Attab syncline using paleomagnetic data. Paleomagnetic studies are particularly useful for deciphering the primary or secondary origin of orogenic curvatures (see e.g. Weil et al., 2013 and references therein), provided that the obtained paleomagnetic vectors correspond to a magnetisation acquired before the orogenic stage (Eldredge et al., 1985; McFadden et al., 1995 among others). Previous paleomagnetic studies show that Jurassic and Cretaceous rocks in the Atlasic belt are remagnetized (Torres-López et al., 2014). In the present work, we will use the results of this remagnetization in Jurassic-Cretaceous sediments to discuss the age of folding and the mechanism responsible for the fold axial shape in the Aït Attab syncline.

2. Geological setting and sampling

The High Atlas is considered an intracontinental chain, resulting from the inversion of previous extensional or transtensional Mesozoic basins related to Triassic and Jurassic rifting (e.g. Mattauer et al., 1977; Rodgers, 1987; Ziegler et al., 1995). The Jurassic extension favoured the development of a mosaic of rhomb-shaped depocenters, limited by synsedimentary anticlines (the so-called anticline ridges, Studer and du Dresnay, 1980; Laville, 1985; Laville et al.,2004). Basin inversion occurred from Cenozoic to recent times (Choubert and Faure-Muret, 1962; Mattauer et al., 1977; Schaer, 1987; Laville, 1988; Jacobshagen et al.,1988; Michard, 1976; Laville and Piqué, 1992; Beauchamp et al., 1996, 1999; Frizon de Lamotte et al., 2000; Gómez et al., 2000; Teixell et al., 2003; Arboleya et al., 2004). Reactivation of extensional faults and folding during inversion resulted in a thick-skinned deformation style, where basement was involved in the compressional deformation (e.g. Frizon de Lamotte et al., 2000; Teixell et al., 2003; El Harfi et al., 2006). Conversely, along the southern border of High Atlasic belt, inversion is associated with thin-skinned tectonics exploiting detachment levels within the Mesozoic sequence (e.g Beauchamp et al., 1999; Benammi et al., 2001; Teixell et al., 2003). The age of the initial inversion is controversial. Some believe that inversion developed during Late Jurassic- Early Cretaceous times, and is represented in the Atlasic belt by small-scale folds and unconformities (e.g. Laville, 1985; Ibouh, 2004; Souhel, 1996; Beauchamp et al., 1996). Conversely, others believe that inversion commenced after post-Early Eocene times (e.g. Frizon de Lamotte et al., 2000; Missenard, 2006).

In the Central High Atlasic chain, regional folds are either large, gentle synclines, containing Middle Jurassic-Cretaceous sediments, or narrow anticlines cored by Liassic limestones (Laville, 1985; Ibouh, 2004). The Aït Attab syncline is filled with Jurassic-Cretaceous terrigenous sedimentary rocks (red beds, Fig.1a). Several studies have established the stratigraphy, biostratigraphy and chronostratigraphy of this red-bed sequence (Haddoumi et al., 2002, 2010; Charrière et al., 2005, 2011; Löwner, 2009; Mojon et al., 2009; Fig.1b). Accordingly, the first group of siltstones and sandstones from the "*couches rouges*" (red beds) defined by Jenny et al. (1981) and considered as infra-Aptian sediments by Rolley (1978) is divided into several units. The first unit of red beds "*sensu stricto*" formed by conglomeratic and red sandstones of the "Guettioua Formation" was ascribed to the Dogger (Bathonian-Callovien). At the top of this formation is a basalt flow level "Horizon B1" dated as Late Jurassic (Haddoumi et al., 2010; Mojon et al., 2009; Charrière et al., 2011; Bensalah et al., 2013). The overlying red pelites and evaporites (Iouaridene Formation) are attributed to the Hauterivian? - Lower Barremian (Mojon et al., 2009; Haddoumi et al., 2010), although the base of this unit is dated as Late Jurassic (Kimmeridgian, Haddoumi et al., 2010). Upward, alternating red sandstones and clays (Jbel Sidal Formation) were interpreted as Barremian (Haddoumi et al., 2002; Charrière et al., 2005; Löwner, 2009). This formation begins with a second basalt flow level, "Horizon B2" attributed to the Early Cretaceous (Haddoumi et al., 2010; Mojon et al., 2009; Charrière et al., 2011). The second group of red beds, deposited above the Aptian marly limestones, characterized by friable sandstones, with some clayey intercalations at its base (Souhel, 1996) was dated as Albo-Cenomanian (Souhel, l996; Löwner, 2009).

A total of 21 sites were sampled, covering the whole Upper Jurassic to Albian-Cenomanian stratigraphic series of the study area (Fig.1b). The sampling was conducted along several profiles across the Aït Attab syncline (Fig.1b). The sampling was done to characterize the paleomagnetic geometry of the target units across the syncline and to ensure a good coverage of the stratigraphic sequence, as a function of outcrop conditions, accessibility and possibility of sampling different rock types. Additionally, a local meter-scale parasitic fold, site ATS, was sampled in both of its limbs in the Bathonian rocks, in order to compare the fold test of both macro and meter-scale structures.

Samples were collected with a portable electric drill machine powered by a gasoline generator. The drill bits were water-cooled during drilling. At every site, the weathered soil (sometimes down to 1 m) was removed to reach fresh fine-grained rocks. At each site, an average of 10 samples was taken. The cores were oriented *in situ* with an inclinometer supplied with a magnetic compass. In the laboratory, the samples were cut to obtain specimens of standard size (2.5 cm in diameter and 2.2 cm in length).

3. Methods

All paleomagnetic and rock magnetic analysis have been performed in the Paleomagnetic laboratory of Burgos University in Spain. The natural remanent magnetization (NRM) of all specimens was first measured on a 2G-755 cryogenic magnetometer. After that, all specimens were subject to stepwise thermal demagnetization using a TD48-SC thermal demagnetizer by 15 to 25 steps. Thermal demagnetization was done in steps of 25ºC (10 to 5°C for some groups of specimens) up to 660-670ºC except for some samples, reaching 685ºC. Representative specimens were subjected to alternating field (AF) demagnetization, following progressive steps until 100mT. The mineralogical changes induced by thermal demagnetization were controlled by measuring the low-field magnetic susceptibility during the demagnetization process using a KLY4S (AGICO Kappabridge). The characteristic magnetic component (ChRM) was isolated using linear regression techniques, and Fischer's (1953) statistics were used to compute the mean directions with the software Remasoft 3.0 (Chadima and Hrouda, 2006).

Selected specimens from different facies and series were used for rock magnetic analysis. The acquisition curves of isothermal remanent magnetization (IRM) were induced in progressively increasing fields up to 2T using a pulse magnetizer M2T-1-Ferronato. Three orthogonal axes IRMs were thermally stepwise demagnetized following the method proposed by Lowrie (1990). Other magnetic mineralogy experiments such as thermomagnetic curves, hysteresis loops with maximum induced field of 1T and back-field experiments were performed with a variable field translation balance (MMVFTB, Petersen Instruments, noise 5 x 10^{-8} Am^2).

4. Paleomagnetic results

In the studied rocks, two different sets of magnetic properties and behaviour were observed and related to their host lithology: the first set involves all red-bed samples collected in the Infra-Aptian and the Albian-Cenomanian at a total of 15 sites, and the second one comprises only Aptian marly limestones from 5 sites. The magnetic susceptibility varies between 200 x 10^{-6} SI units for the red beds and 60 x 10^{-6} S.I. units for the white marly limestones (see also Moussaid et al., 2013) and the intensity of the natural remanent magnetization (NRM) displays values from 3 x 10^{-2} A/m in the red beds to 3 x 10^{-4} A/m in the marly limestones.

The thermal demagnetization diagrams of all samples belonging to the “red beds group” show a stable directional component of normal polarity with unblocking temperatures comprised between 250ºC and 550ºC in some cases (Fig. 2c, e) or up to 650ºC (Fig. 2a). This component is considered to be the characteristic remanent magnetization (ChRM). Sometimes, this magnetic directional component is formed by two magnetic phases evidenced by two drops in the NRM intensity diagram, the first one between 500ºC and 610 ºC (Fig. 2c) and a second at 650ºC (Fig. 2c, e). Samples were not demagnetized after peak fields of 100 mT (Fig. 2d, i). The observed maximum unblocking temperatures and the AF demagnetization of these samples suggest a high coercivity phase with hematite as the main magnetic mineral carrier. A higher temperature reversed component was observed, with unblocking temperatures higher than 650ºC, in a few cases in the red beds sites (Fig. 2b, f). A directional analysis of this component was inconclusive due to the scarcity of data, preventing an outcome with statistical significance.

The marly limestones show three behaviours on the basis of the demagnetization of the natural remanent magnetization (NRM). Unfortunately, most samples do not give a reliable directional component. Sites AT12 and AT20 show negligible intensity of magnetization after demagnetized at 250ºC, whereas sites AT14, AT8 and AT6 show a very low unblocking temperature component (100ºC) probably due to the presence of goethite (Fig. 2j), according to the high coercivity shown by these samples after 100 mT AF demagnetization (Fig. 2k). At higher temperatures, no reliable magnetic components were observed. Only the grey marly specimens of AT10 site show a stable component with maximum unblocking temperatures ranging between 550 and 620ºC (Fig. 2l). The NRM intensity diagram displays a slight decrease about 500 to 550°C and a strong decline around 620 to 640°C. The AF demagnetization of a representative sample of site AT10 shows low to medium coercivities for this component indicating that probably magnetite contributes to the magnetization (Fig. 2m).

5. Rock magnetism results

Red beds show hysteresis loops without magnetic saturation, due to the presence of high coercivity minerals (Fig. 3a, c and e). The thermomagnetic curves display a sharp drop when heating about 680°C, corresponding to the Curie temperature of hematite as high coercivity phase in the red beds group (Fig. 3b, d). In addition, wasp-waisted hysteresis loops occur in all analyzed samples. This kind of hysteresis shape usually indicates the presence of mixture of ferromagnetic minerals with high and low coercivity magnetic phases or mixture of different grain sizes of a single magnetic mineral (Roberts et al., 1995; Tauxe et al., 1996). The wasp-waisted shape of hysteresis loop is especially remarkable in AT15 selected specimen (Fig. 3e). These results are confirmed by the IRM acquisition and 3D IRM demagnetization (Fig. 4). The IRM spectrum of the red beds group displays an increase of the magnetization, without saturation at the maximum applied field (2T, Fig. 4b). The corresponding 3D IRM diagram shows a clear drop in the hard (2T) and medium (0.4T) phases at around 680°C. The soft phase (0.12T) displays very low magnetization values and reaches the zero axis around 580°C. This result indicates the dominance of haematite and the presence of a small quantity of magnetite (Fig. 4a). The coexistence of these two minerals is well defined in site AT15 given the above mentioned wasp-waisted curve (Fig. 3e) and the two clear drops of 580ºC and 680ºC in the thermomagnetic heating curve (Fig. 3g). In addition, the back field (that shows an inflexion point at 50 mT), IRM acquisition and 3D IRM demagnetization (Fig. 4e and f) also indicate the presence of these two magnetic phases. For almost all specimens from the red beds group, the heating-cooling curves are reversible, indicating the absence of new magnetic minerals created during heating, except for the AT15-6b, which displays a strong increase of magnetization when cooling.

The marly limestones display two magnetic behaviours on the basis of their ferromagnetic characterization. In the first one, illustrated by the AT6-12 specimen from the Aptian limestones, the hysteresis loops do not show saturation, thus indicating the presence of high coercivity minerals. Wasp-waisted shape observed in the hysteresis loop evidences the mixture of different coercivity magnetic phases (Fig. 3h). This mixture is clearly observed in the thermomagnetic curves of this specimen, displaying two drops of the magnetization spectrum. The first one is an important decrease at around 80 to 100°C, attesting the presence of goethite. The second decline is slight and progressive until 580 to 600°C, perhaps indicating the likely presence of magnetite. The IRM acquisition and 3D IRM demagnetization of the AT10-9 also from the Aptian marly limestones show the presence of two phases (Fig. 4c, d). The hard phase spectrum (2T) displays a sharp drop around 680°C (Fig. 4c) indicating that the high coercivity phase is hematite, while the soft phase (0.12) spectrum shows a sharp drop around 580°C (Fig. 4c), consistent with the Curie temperature of the magnetite as low coercivity mineral.

The second behavior observed in marly limestones is shown by AT10.6a specimen, from the Aptian gray marly facies. In this case, the hysteresis loop is linear indicating the dominance of paramagnetic minerals (Fig. 3j). The corresponding thermomagnetic curves exhibit a gradual decrease of magnetization when heating, with very low values of magnetization. The magnetization increases strongly around 400 or 450°C, and may be linked to the formation of new magnetic phases due to transformation of paramagnetic minerals to magnetite as is evidenced by the Curie temperature of 580ºC observed in the heating curve (Fig. 3k). AT2-8 from red- yellowish facies, shows nearly saturated spectrum, and can be related to the dominance of low coercivity minerals. This behavior was also observed in the thermal demagnetization of 3D IRM spectra of this sample; therefore the soft phase curve (0.12 T) shows a maximum unblocking temperature of 580°C, indicating that magnetite is the main ferromagnetic mineral (Fig. 4g, h). There is also a “high coercivity phase" with maximum unblocking temperatures of 680°C and magnetic coercivities between 0.4T and 2T (Fig. 4g), consistent with the presence of haematite.

6. Directional analysis

The ChRM was systematically defined in 11 sites in red bed sites and only one site (AT10) in marly limestones (Table 1, Fig. 5). The other 8 sites sampled in marly limestones do not show a stable component, as previously described in the NRM result section. All directions, before and after tectonic corrections, show systematically normal polarities, in all outcrops from Bathonian to Albian-Cenomanian (Table 1). Taking into account that both polarities are expected for Jurassic and Early Cretaceous ages, this evidence is a first sign that the ChRM is a secondary magnetization.

A regional fold test with all site means of the ChRM was performed, except for site ATS to infer the age of remagnetization in relation to the Aït Attab syncline formation (Fig. 5). The grouping of mean site directions increases strongly after bedding correction (Fig. 5). This result indicates that the fold test is positive, and the remagnetization is pre-folding. We have used the McFadden and Jones (1981) method to test the statistical confidence of the fold test. All sites were divided in two groups, the first one concerning the North limb of the syncline and the second one regrouping all sites taken in its southern flank. Before tectonic correction, the parameter $f > F$ (F is the value of f at a 95% level of confidence) whereas after tectonic correction, $f < F$, thus resulting a positive fold test at the 95% level of confidence (Table 2). This result evidences for the first time that the observed remagnetization was acquired before the folding of the Aït Attab syncline in the sampled area.

Although not very common, metre-scale intraformational folds cut at their top by local unconformities are present in sediments filling the Aït Attab basin (Fig. 6a,b). To better constrain the relative age of the ChRM and reinforce the evidence for its secondary origin, we sampled the two limbs of one of these folds in Bathonian beds to perform a fold test (site ATS). In this case, the fold test is negative, indicating that the magnetization was acquired after synsedimentary folding (Fig. 6c, d). The McFadden and Jones (1981) statistical fold test performed with sample directions in this small fold gives parameters $f < F$ before tectonic correction and $f > F$ after bedding correction. This result indicates that the magnetization is post-folding with a level of confidence of 95% (see table 2). Therefore, we conclude that: 1) the ChRM displays systematically normal polarity directions in all sites taken in different formations in age and facies, indicating that it is a secondary magnetization; 2) the regional fold test performed in the Aït Attab syncline is positive at the 95% level of confidence proving that the remagnetization was acquired before this structure; and 3) a fold test performed in a metre-scale syn-sedimentary fold affecting Bathonian rocks provides a post-folding result reinforcing that the ChRM is a remagnetization.

7. Discussion

7.1. Timing of remagnetization

The study of paleomagnetic directions obtained from sites in the Aït Attab syncline reveals that the magnetization of Upper Jurassic and Lower Cretaceous sedimentary rocks is dominated by a remagnetization of normal polarity. This remagnetization was acquired after the formation of syn-sedimentary Bathonian structures and predates the regional folding of the Aït Attab syncline. The mean direction calculated for this remagnetization is D= 331.1º;

I= 40.9º with k = 91.6 and α_{95} = 4.6º. To define the age of this remagnetization, we compare its inclination and declination with the expected declinations and inclinations for the African plate using the Global Apparent Polar Wander Path (GAPWP) in African coordinates as determined by Torsvik et al. (2012), and as proposed for the remagnetization direction obtained in the Jurassic series of the Imilchil area (~60 km to the east of the study area) by Torres-López et al. (2014) (Fig. 7). This comparison is reliable as no vertical-axis rotations seem to occur in the studied area based on structural evidence. Overall, the intersection between the inclination line of the remagnetization found in the Aït Attab syncline and the inclination curves of APWP of Africa cover a wide band of ages (Fig. 7a). Conversely, the comparison between the declination of the Aït Attab ChRM components and the synthetic GAPWP only shows three possible solutions: the first one is around 100-110 Ma (Albian-Cenomanian), the second one around 160 Ma (Middle to Late Jurassic), and the third one around 240 Ma (Late Triassic, see Fig.7b). Regardless of rock age, lithological variations and magnetic carriers, consistent directions of normal polarity are observed in all samples, supporting the hypothesis of a unique event affecting the entire sedimentary sequence that was deposited between the Jurassic and Cretaceous. Taking this constraint into account, the second (160 Ma) and third (240 Ma) solutions would not be possible and consequently the remagnetization in the Aït Attab area was probably acquired for an age ranging between 95Ma and 117 Ma (Albian-Cenomanian). This age fits with the Cretaceous Normal Polarity Superchron, explaining the systematically normal polarity registered in all samples. In addition, this result is consistent with a post-folding acquisition observed in the syn-sedimentary Bathonian structure (site ATS). These results also fit with recent data by Torres-López et al. (2014), who argue that the Cretaceous remagnetization observed in the Imilchil area (Eastern Central High Atlas) corresponds to a regional event.

7.2. Age of folding of the Aït Attab syncline

The interpretation of folding being post the inferred Albian-Cenomanian remagnetization has important implications for understanding High Atlas tectonics, as this result excludes the possibility of an Early Cretaceous compressional event being responsible for the formation of large folds in the Aït Attab syncline area. These folds are thus probably attributed to the Cenozoic compressional tectonics (e.g. Michard et al., 2008).

On the other hand, the result of the fold test for the small intra-formational fold (ATS), indicates that these structures predate the remagnetization. This evidence would support an interpretation that the small folds and unconformities observed in the Aït Attab area are linked to an earlier Jurassic-Lower Cretaceous tectonic event, for which evidence is postulated to exist in the axial zone of the Central High Atlas (Laville, 1985; Laville and Piqué, 1992; Ibouh, 1994, 2004). However, this interpretation is preliminary as it is based on data from a single location within a single map-scale fold in the Central High Atlas.

7.3. Curved geometry of the Aït Attab syncline

The principal aim of this work is to use paleomagnetic data to discuss the origin of the curved shape of the Aït Attab syncline, that shows an eastern segment with E-W trend and a western part with a NE-SW oriented axis (Figs. 1, 8). Based in structural data, Beauchamp (2004) interpreted this syncline as a typical curved fold in the Central High Atlas, linked to the superimposed folding in the Afourer–Jbilet area. The E-W direction (f1) was considered the result of a first folding stage, subsequently refolded by a second folding event with NW-SE trend (f2). The Aït Attab syncline and similar structures have also been explained to be the result of reactivation/inversion of previous extensional basement faults. The NE-SW Mesozoic cover structures would be distorted, producing curved folds, with axial curvature leading to the formation of “S” and “Z” shape structures (Ibouh et al., 2001; Ibouh, 2004).

In the light of paleomagnetic data, the comparison between the two segments of the Aït Attab syncline (Fig. 8a) indicates that all paleodeclinations are parallel and show the same direction. An oroclinal bending test (Fig. 8b) shows no correlation between paleodeclinations and strike direction (negative test), indicating that the curved geometry in plan view of the Aït Attab syncline does not correspond to an oroclinal bending structure *sensu stricto* (Weil and Sussmann, 2004). This result is also consistent with magnetic lineation encountered in the Aït Attab area (Moussaid et al., 2013).

According to our results and interpretations, we can infer that the current curved shape in plan view of the Aït Attab syncline is primary and, therefore, is not the result of subsequent distortion of a NE-SW trending Atlasic structure formed during the Cenozoic inversion. This curved geometry cannot be explained by superimposed folding and therefore, with older E-W folds being refolded by NW-SE trending folds. The Aït Attab syncline is not an oroclinal bend. Consequently, the Aït Attab geometry is an originally curved structure postdating a remagnetization during Albian-Cenomanian times.

Consequently, the curved geometry of the Aït Attab syncline in plan view must be considered as primary. We infer its shape to result from an inheritance of its Mesozoic basinal geometry, namely the existence of faults oriented N045°-N070° and N090° moving under an extensional/transtensional regime during the Mesozoic (Fig. 9). These faults were responsible for the rhomb-shaped geometry of depocenters and the opening of pull-apart basins in the Central High Atlas (Laville et al., 2004). Taking into account the overall shortening direction in the High Atlas, the E-W folds can be linked to the Cenozoic inversion (N-S shortening), while the NE-SW trends are controlled by the basement faults trends (Fig.9).

8. Conclusion

Jurassic-Cretaceous rocks in the Ait Attab syncline of the Central High Atlas show a widespread remagnetization with a characteristic component that shows normal polarities in all samples. The mean calculated direction after tectonic corrections coincides with the widespread remagnetization described by other authors (Torres-López et al., 2014) in the High Atlas, interpreted as occurring in Albian-Cenomanian times (approximately 105 Ma, according to the APWP of Africa), assuming that no vertical axes rotations occurred in the area. The rock magnetic studies show that haematite is the main carrier of the remagnetization in the red beds but magnetite is also the carrier of remagnetization in some sites. Goethite is also present in some limestone samples where remagnetization was not observed.

According to the structural interpretations and the fold test results, this remagnetization post-dates synsedimentary Bathonian structures and predates the formation of the Aït Attab syncline. Folding of the Aït Attab syncline can be, therefore, considered as post-Albian-Cenomanian, probably related to the Cenozoic tectonism, when basin inversion occurred in the High Atlas. The comparison of paleodeclinations between the two segments of the Aït Attab syncline axis, with different structural trends but similar paleomagnetic trends, reveals a result consistent with hypothesis postulating that the present curved geometry can be considered primary, possibly influenced by the geometry of the previous extensional or transtensional Jurassic-Cretaceous basin underlain by NE-SW and E-W oriented basement faults.

ACKNOWLEDGEMENTS

Funding for this work came from projects, CGL2009-10840, CGL2009-08969 and CGL2012-38481 of the Dirección General de Investigación Científica y Técnica, Ministerio de Economía y Competitividad of the Spanish government and European Regional Development Fund. The authors thank Gabriel Gutiérrez Alonso and Daniel Pastor Galán for constructive reviews of the manuscript. We thank also William Dunne for his suggestions that helped to improve this paper.

REFERENCES

Arboleya, M.L., Teixell, A., Charroud, M., Julivert, M., 2004. A structural transect through the High and Middle Atlas of Morocco. Journal of African Earth Sciences 39, 319-327.

Beauchamp, W., Barazangi, M., Demnati, A., El Alji, M., 1996. Intracontinental rifting and inversion: Missour Basin and Atlas Mountains, Morocco. AAPG Bull. 80, 1459-1482.

Beauchamp, W., Allmendinger, R.W., Barazangi, M., Demnati, A., El Alji, M., Dahmani, M., 1999. Inversion tectonics and the evolution of the High Atlas mountains, Morocco, based on a geological-geophysical transect. Tectonics 18, 163-184.

Beauchamp, W., 2004. Superposed Folding Resulting from Inversion of a Synrift Accommodation Zone, Atlas Mountains, Morocco. In K. R. McClay, ed., Thrust tectonics and hydrocarbon systems: AAPG Memoir 82, 635-646

Benammi, M., Arbi Toto, E., et Chakiri, S., 2001. Les chevauchements frontaux du haut atlas central marocain : styles structuraux et taux de raccourcissement différentiel entre les versants nord et sud : On the differential structural styles and rates of shortening on the northern and southern bordering thrusts of the Moroccan Central Atlas. Comptes rendus de l'Académie des Sciences-Series IIA-Earth and Planetary Sciences, 333 (4), 241-247.

Bensalaha M.K, Youbi N., Mata J., Madeira J., Martins L., El Hachimi H., Bertrand H., Marzoli A., Belleini G., Doblas M., Font E., Medina F., Mahmoudi A., Berâouz E., Miranda R., Verati C., De Min A., Ben Abbou M., Zayane R., 2013. The Jurassic–Cretaceous basaltic magmatism of the oued El-Abid syncline (High Atlas, Morocco): Physical volcanology, geochemistry and geodynamic implications. Journal of African Earth Sciences, 81, 60–81.

Chadima, M., Hrouda, F. 2006. Remasoft 3.0 a user-friendly paleomagnetic data browser and analyzer. Travaux Géophysiques, XXVII, 20-21.

Charrière, A., Haddoumi, H., Mojon, P-O., 2005. Découverte de Jurassique supérieur et d'un niveau marin du Barrémien dans les «couches rouges» continentales du Haut Atlas central marocain: implications paléogéographiques et structurales. C. R. Palevol, 4, 385-394.

Charrière, A., Ibouh, H., Haddoumi, H., 2011. Circuit C7, Le Haut Atlas central de BeniMellal à Imilchil. In Michard et al. (Eds.), Nouveaux guides géologiques et miniers du Maroc, vol. 7, Notes Mém. Serv. géol. Maroc, n° 559, 109-162.

Choubert, G., Faure-Muret, A., 1962. Evolution du domaine atlasique marocain depuis les temps paléozoieques, livre à la mémoire du Prof. P. Fallot. Mémoire hors-série service de la Société géologique de France 1, 447-514.

El Harfi, A., Guiraud, M., Lang, J., 2006. Deep-rooted ‘‘thick skinned’’ model for the High Atlas Mountains (Morocco). Implications for the structural inheritance of the southern Tethys passive margin. Journal of Structural Geology 28(11), 1958-1976.

Eldredge, S., Bachtadse V., and van der Voo R., 1985. Paleomagnetism and the orocline hypothesis: Tectonophys-ics, 119, p. 153 – 179

Frizon de Lamotte, D., Leturmy, P., Missenard, Y., Khomsi, S., Ruiz G., Saddiqi O., Guillocheau F., Michard A., 2009. Mesozoic and Cenozoic vertical movements in the Atlas system (Algeria, Morocco, Tunisia): An overview. Tectonophysics, 475, 9–28.

Frizon de Lamotte, D., Saint Bézar B., Bracène R., Mercier E., 2000. The two main steps of the Atlas building and geodynamics of the western Mediterranean. Tectonics, 19, 740-761.

Giese, P., Jacobshagen, V., 1992. Inversion tectonics of intracontinental ranges : High and Middle Atlas, Morocco. Geo.Rundsch., 81, 249-259.

Gomez, F., Beauchamp, W., Barazangi, M., 2000. Role of the Atlas mountains (northwest Africa) within the African-Eurasian plate-boundary zone. Geology, 28, 775–778.

Guiraud, R., Binks, R.M., Fairhead, J.D., Wilson, M., 1992. Chronology and geodynamic setting of Cretaceous-Cenozoic rifting in West and Central Africa. In: Ziegler, E.A. (Ed.), Geodynamics of Rifting. Vol. II. Case History studies on Rifts: North and South America, Africa-Arabia. Tectonophysics, 21, 227-234.

Guiraud, R., Bosworth ,W., Thierry, J., Delplanque, A., 2005. Phanerozoic geological evolution of the Northern and Central Africa: An overview. Journal of African Earth Sciences-Phanerozic Evolution of Africa, 43 (1-3), 83-143.

Haddoumi, H., Charrière, A., Feist, M., Andreu, B., 2002. Nouvelles datations (Hauterivien supérieur- Barrémien inférieur) dans les "couches rouges" continentales du Haut Atlas central marocain; conséquences sur l'âge du magmatisme et des structurations mésozoïques de la chaîne Atlasique. C R Palevol 1, 259-266.

Haddoumi, H., Charrière, A., Mojon, P.O., 2010. Stratigraphie et sédimentologie des «Couches rouges» continentales du Jurassique-Crétacé du Haut Atlas central (Maroc): implications paléogeographiques et géodynamiques. Geobios, 43, 433–451.

Ibouh, H, El Bchari, F., Bouabdelli, M., Souhel, A., Youbi, N.E., 2001. L'accident Tizal-Azourki: Haut Atlas central (Maroc). manifestations synsédimentaires liasiques en extension et conséquence du serrage atlasique. Estudios Geologicos, 57, 1-2, 15-30.

Ibouh, H., Bouabdelli, M., Zargouni, F., 1994. Indices de tectonique synsédimentaire dans les dépóts aaléno-bajocien de la région d 'Imilchil (Haut Atlas Central, Maroc). Miscellanea Servo Geol. Naz. Roma, 5, 305-310.

Ibouh H., 2004. Du rift avorté au bassin sur décrochement, contrôles tectonique et sédimentaire pendant le Jurassique (Haut-Atlas central, Maroc).Thèse d'état Es-Sciences. Université Cadi Ayyad, Marrakech, 224 p.

Jacobshagen, V., Brede, R., Hauptmann, M., Heinitz, W., Zylka, R., 1988. Structure and post-Paleozoic evolution of the Central High Atlas, in Jacobshagen V. (Ed.), The Atlas system of Morocco. Lect. Notes Earth Sci. 15, 245-271.

Jenny, J., Le Marrec, A., Monbaron, M., 1981. Les Couches Rouges du Jurassique moyen du Haut Atlas central (Maroc): corrélations lithostratigraphiques, éléments de datation et cadre tectono-sédimentaire, Bull. Soc. géol. Fr. (7) 23, 627-639.

Kent, D.V., 1988. Further paleomagnetic evidence for oroclinal rotation in the central folded Appalachians from the Bloomsburg and the Mauch Chunk Formations. TECTONICS, 7,749-759.

Laville, E., 1985. Evolution sédimentaire, tectonique et magmatique du Bassin jurassique du Haut Atlas (Maroc): modèle en relais multiples de décrochements, Unpubl. Thesis Univ. Sci. Techn. Languedoc Montpellier, 166.

Laville, E., Piqué, A., 1992. Jurassic penetrative deformation and Cenozoic uplift in the central high atlas (Morocco): a tectonic model. Structural and orogenic inversions. Geologische Rundshau, 81, 1, 157-170.

Laville, E., Piqué, A., Amrhar, M., et Charroud, M,. 2004. A restatement of the Mesozoic Atlasic Rifting (Morocco). Journal of African Earth Sciences, 38 (2), 145-153.

Laville, E., 1988. A multiple releasing and restraining stepover model for the Jurassic strike-slip basin of the Central High Atlas (Morocco). In: Manspeizer, W. (Ed.), Triassic–Jurassic rifting. Continental Breakup and the origin of the Atlantic Ocean and passive margins, Part I. In: Developments in Geotectonics, 22. Elsevier, New York, pp. 499–523

Löwner, R., 2009. Recherches sédimentologiques et structurales à l'articulation entre le Haut Atlas et Moyen Atlas et la Haute Moulouya , Maroc, 201p.

Lowrie, W., 1990. Identification of ferromagnetic minerals in a rock by coercivity and unblocking temperature properties. Geophys. Res. Lett., 17, 159-162.

Marshak, S., 1988. Kinematics of orocline and arc formation in thin-skinned orogens. Tectonics, 7, 73-86.

Mattauer, M., Tapponier, P., Proust, F., 1977. Sur les mécanismes de formation des chaînes intracontinentales .L'exemple des chaînes atlasiques du Maroc. Bull. Soc. géol. Fr. (7) 19, 521-526.

McFadden, P. L., Jones, D. L., 1981. The fold test in palaeomagnetism, Geophys. J. R. astr. Soc., 67, 53-58.

MacFadden, B. J., Anaya F., and Swisher C. C., 1995. Neogene paleomagnetism and oroclinal bending of the central Andes of Bolivia, J. Geophys. Res., 100,8153-8167.

Michard, A., 1976. Eléments de géologie marocaine. Notes Mém. Serv. géol. Maroc 252, 408pp.

Michard, A., Frizon de Lamotte, D., Liégeois, J.-P., Saddiqi, O., Chalouan, A., Roure, F., 2008. Conclusion: continental evolution in western Maghreb. In: Michard, A.,Saddiqi, O., Chalouan, A., Frizon de Lamotte, D. (Eds.), Continental Evolution: The Geology of Morocco. Springer Verl., Berlin, Heidelberg, pp. 395–404.

Mojon, P-O., Haddoumi, H., Charrière, A., 2009. Nouvelles données sur les Charophytes et Ostracodes du Jurassique moyen-supérieur - Crétacé inférieur de l'Atlas marocain. Carnets de Géologie / Notebooks on Geology, Brest, Mémoire 2009/03 (CG2009-M03), 1-39.

Moussaid B., El Ouardi H., Casas-Sainz A., Villalaín J.J., Román-Berdiel T., Oliva-Urcia B., Soto R., Torres-López S., 2013. Magnetic fabrics in the Jurassic–Cretaceous continental basins of the northern part of the Central High Atlas (Morocco): Geodynamic implications. Journal of African Earth Sciences, 87, 13-32.

Roberts, A. P., Cui, Y., Verosub, K. L., 1995. Waspwaisted hysteresis loops: Mineral magnetic characteristics and discrimination of components in mixed magnetic systems, J. Geophys. Res., 100, 17,909 – 17,924.

Rodgers, J., 1987. Chains of basement uplifts within cratons marginal to orogenic belts. Am. J. Sci., 287, 661–692.

Rolley, J.-P., 1978. Carte géologique du Maroc au 1/100.000 : feuille d‟Afourer. Notice explicative. Notes et Mémoires du Service Géologique du Maroc, Rabat 247, 247 bis, 1–103.

Schaer, J. P., 1987. Evolution and structure of the High Atlas of Morocco, inThe Anatomy of Mountain Ranges, edited by J. P. Schaer and J. Rodgers, pp. 107–127, Princeton Univ. Press, Princeton, N. J.

Schwartz, S.Y., Van der Voo, R., 1983. Paleomagnetic evaluation of the orocline hypothesis in the central and southern Appalachians: Geophysical Research Letters, 10, 505–508.

Souhel, A., 1996. Le Mésozoïque dans le Haut Atlas de Béni-Mellal (Maroc). Thèse d'Etat, Univ. Cadi Ayyad, Fac. Sci. Marrakech, 235p.

Tauxe, L., Mullender, T. A. T., Pick, T., 1996. Pot-bellies, wasp-waists and superparamagnetism in magnetic hysteresis. J. Geophys. Res., 101, 571– 583.

Teixell, A., Arboleya, M-L., Julivert, M., Charroud, M., 2003. Tectonic shortening and topography in the central High Atlas (Morocco). Tectonics 22, 5, 13.

Torres, S., Villalaín, J.J., Casas, A., El Ouardi, H., Moussaid B., Ruiz-Martínez V.C., 2014. Widespread Cretaceous secondary magnetization in the High Atlas (Morocco). A common origin for the Cretaceous remagnetizations in the western Tethys? Journal of the Geological Society, London.

Torsvik, T. H., Van der Voo, R., Preden, U., Mc Niocaill, C., Steinberger, B., Doubrovine, P. V., Van Hinsbergen, D., Domeier, M., Gaina, C., Tohver, E., Meert, J.G., McCausland, P.J.A., Cocks, L.R.M. 2012. Phanerozoic polar wander, palaeogeography and dynamics. Earth-Science Reviews, 114, 325-368.

Weil A. B., Gutiérrez-Alonso G., Johnston S.T., Pastor-Galán D., 2013. Kinematic constraints on buckling a lithospheric-scale orocline along the northernmargin of Gondwana: A geologic synthesis. Tectonophysics 582, 25–49.

Weil, A.B., Sussman, A., 2004. Classifying curved orogens based on timing relationships between structural development and vertical-axis rotations. Geological Society of America Special Paper 383, 1–17.

Ziegler, P.A., Cloetingh, S., van Wees J-D., 1995. Dynamics of intra-plate compressional deformation: the Alpine foreland and other examples. Tectonophysics, 252, 7-59.

Figure Captions

Figure 1. (a)Location of study area within the High Atlas belt and geological map of the Aït Attab syncline with sample sites AT1 to AT20. The ATS site (a small-scale fold structure) is also shown. (b) Stratigraphical column of the main Jurassic-Cretaceous units in the Aït Attab area (after Mojon et al., 2009).

Figure 2. Zijderveld diagrams of representatives AT specimens in geographic coordinates. Solid symbols indicate projections of vector end points onto the horizontal plane, and the open symbols onto the vertical plane. The corresponding plot of the evolution of normalized NRM intensity (M/Mmax) during the thermal demagnetization was plotted for each example. (k, m, d, i) to show representative AF demagnetization.

Figure 3. Hysteresis loops after (a, c, e, h) and before (j) slope corrections of representative AT specimens. (b, d, f, i, k) thermomagnetic curves of the same specimens with heating (red) cooling (blue) paths. (g and l) represent the detailed view of the heating path of f and k, respectively.

Figure 4. IRM acquisition diagrams (b, d, f, h) and unblocking temperature spectra of three orthogonal IRM components (Mx: 0.12 T; My: 0.4T; Mz: 2T) (a, c, e, g) of representative AT samples. (f) represents an example of IRM and back-field diagram showing the presence of two magnetic phases.

Figure 5. Equal-area projections displaying specimen directions (small circles; with solid symbols corresponding to the directions plotted in the lower hemisphere and open symbols in

the upper hemisphere). The grey circles represent the Aït Attab site mean directions encircled by the confidence area 95% before and after bedding corrections (B.C).

Figure 6. (a) Sampled small-scale folds in the southern limb of the Aït Attab syncline (ATS site); and (b) intraformational folds in equivalent beds in the northern limb of the Aït Attab syncline showing small unconformities within the same sequence to demonstrate their syn-sedimentary origin. Comparison of the regrouping of the specimen ChRM directions in both limbs of the small fold displayed in (a), before (c) and after (d) bedding corrections.

Figure 7. (a) Inclination-age curve; and (b) Declination-age curve expected in the Imilchil area from GAPWP in African coordinates (Torsvik et al., 2012). Uncertainties of the expected directions are shown. The horizontal lines represent the observed inclination/declination (and their uncertainties) at the Imilchil cross-section. The frames with solid lines indicate the possible solutions (modified from Torres et al., 2014).

Figure 8. a) Paleodeclinations by sites plotted on the geological map for the Aït Attab syncline. b) The oroclinal bending test using the declination of all sites considered in this work. Triangles in a) and bars in b) represent the declination error calculated as $\Delta D = \alpha_{95}/\cos I$.

Figure 9. Sketch showing the proposed model for the formation of the primary curvature of the Aït Attab syncline. (a) Structures active during the basinal and (b) compressional stages are approximately plotted on the relief map of the area. (a) Opening of sub-basins in extensional/transtensional regime during the Mesozoic. (b) The basement faults control of map-scale fold geometry during the inversion (Cenozoic) stage.

Table1. Paleomagnetic results of Ait Attab syncline sites

					In Situ				After tilt corrections			
Site	Age	Facies	n	N	D	I	K	α 95	D	I	K	α 95
AT1	Bathonian	red silts and sandestones	8	7	331.9	1.4	20.3	13.7	329.6	43.1	20.3	13.7
AT3	Infra-aptian	red silts and sandestones	8	8	331.7	25.4	103.5	5.5	319	42.1	103.5	5.5
AT4	Infra-aptian	red silts and sandestones	8	8	341.2	17.7	60.9	7.2	337	43.9	45.9	8.3
AT5	Infra-aptian	red silts and sandestones	8	7	329.3	19.5	39	9.8	322.8	38.2	38.8	9.8
AT7	Albo-cenomanian	red silts and sandestones	7	5	327.6	31.8	195.4	5.5	330.3	34.4	197.5	5.5
AT10	Aptian	marls and limestones	8	8	317.9	51.1	83.7	6.1	330.2	30.2	82.5	6.1
AT13	Albo-cenomanian	red silts and sandestones gypsiferous	8	8	339.4	36.8	47.7	8.1	323.4	44.8	47.9	8.1
AT15	Infra-aptian	red silts and sandestones	8	8	329.8	-15	66.4	6.8	345.2	42.8	66.5	6.8
AT17	Infra-aptian	red silts and sandestones	8	6	352	60.2	44.6	10.1	339.2	44.8	44.5	10.2
AT18	Infra-aptian	red silts and sandestones	8	7	337.4	50.6	41.2	9.5	329.7	32.5	41.3	9.5
AT19	Infra-aptian	red silts and sandestones	8	7	329.7	25.9	42.2	9.4	323.6	44.1	42	9.4
AT16	Bathonian	red silts and sandestones	7	6	1.8	60.6	65.4	8.3	298.4	65.7	65.38	8.3
								**	345.6	46.8	65.3	8.4
ATS1	Bathonian	red silts and sandestones	7	7	1.7	53.1	162.79	4.7	334.8	16.3	165.19	4.7
ATS2	Bathonian	red silts and sandestones	5	5	358.6	48.4	149.34	6.3	24.4	43.2	149.12	6.3

**: AT 16 results with regional tectonic corrections using AT17 neighbouring site strike and dip data.

n: number demagnetized samples. N: number of specimens using in this work. D: declination. I: inclination. K and α95, Fisher statistical parameters (Fisher, 1953).

Aït Attab syncline							
In situ	N	D	I	k	α_{95}	f	F_{95}
	12	334.3°	31.1°	11.2	5	1.438	0.350
After tectonic corrections	N	D	I	k	α_{95}	f	
	12	331.1°	40.9°	91.6	4.6	0.091	
Site ATS; small scale folded structure (intraformational folding)							
In situ	N	D	I	k	α_{95}	f	F_{95}
	12	0.3°	51.2°	146.0	3.6°	0.143	0.350
After tectonic corrections	N	D	I	k	α_{95}	f	
	12	351.8°	29.5°	97	14.7°	14.600	

Table 2. McFadden and Jones (1981) fold tests using the results of the Aït Attab syncline limbs and those of the synsedimentary folded structure.

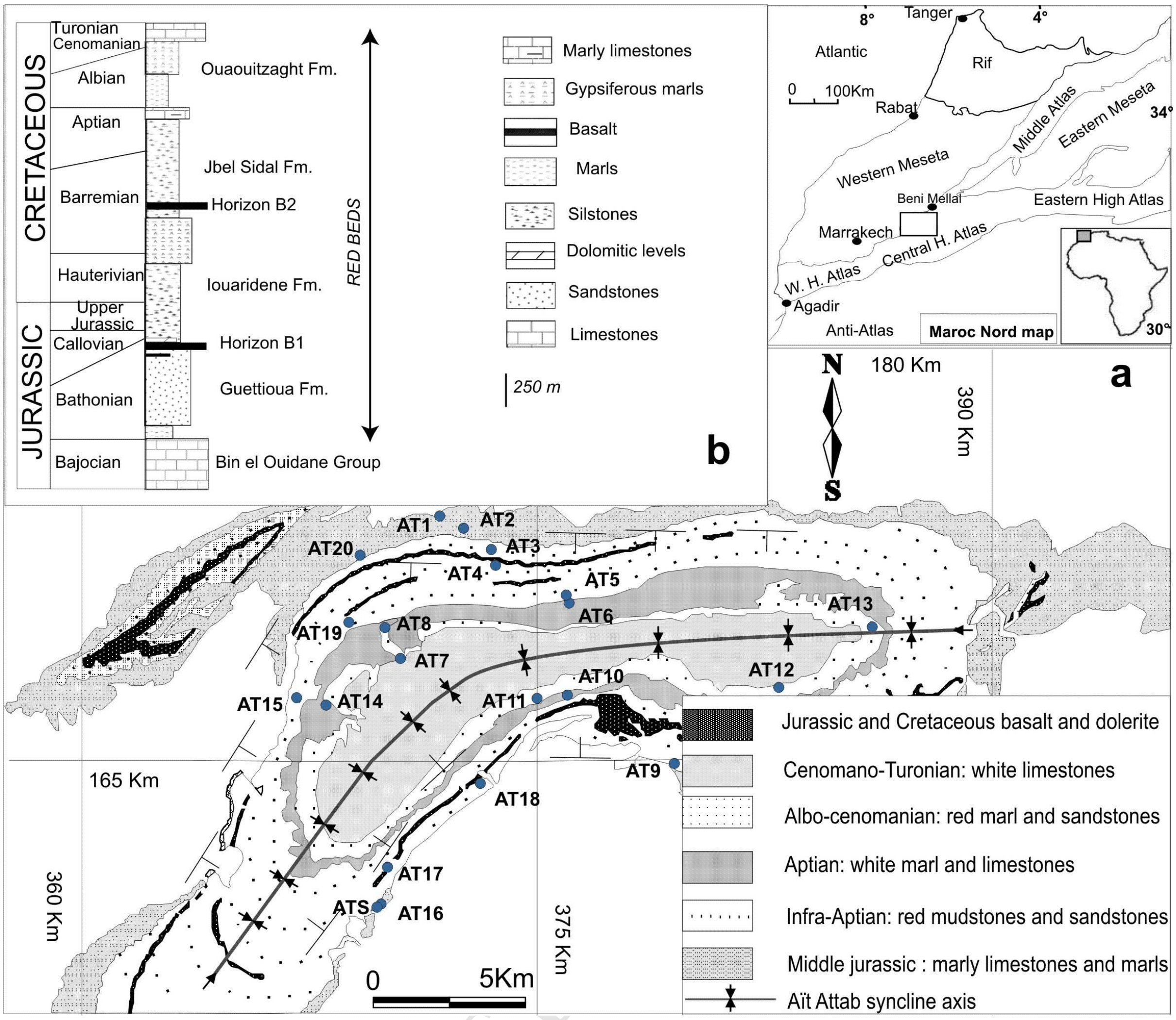
CRETACEOUS
JURASSIC
Turonian
Cenomanian
Albian
Aptian
Barremian
Hauterivian
Upper Jurassic
Callovian
Bathonian
Bajocian
Ouaouitzaght Fm.
Jbel Sidal Fm.
Horizon B2
Iouaridene Fm.
Horizon B1
Guettioua Fm.
Bin el Ouidane Group
RED BEDS
Marly limestones
Gypsiferous marls
Basalt
Marls
Silstones
Dolomitic levels
Sandstones
Limestones
250 m
b
Tanger
8°
4°
Atlantic
Rif
0 100Km
Rabat
34°
Middle Atlas
Eastern Meseta
Western Meseta
Beni Mellal
Eastern High Atlas
Marrakech
Central H. Atlas
W. H. Atlas
Agadir
Anti-Atlas
Maroc Nord map
30°
N
S
180 Km
390 Km
a
AT1
AT2
AT3
AT4
AT5
AT6
AT7
AT8
AT9
AT10
AT11
AT12
AT13
AT14
AT15
AT16
AT17
AT18
AT19
AT20
ATS
165 Km
360 Km
375 Km
0
5Km
Jurassic and Cretaceous basalt and dolerite
Cenomano-Turonian: white limestones
Albo-cenomanian: red marl and sandstones
Aptian: white marl and limestones
Infra-Aptian: red mudstones and sandstones
Middle jurassic : marly limestones and marls
Aït Attab syncline axis

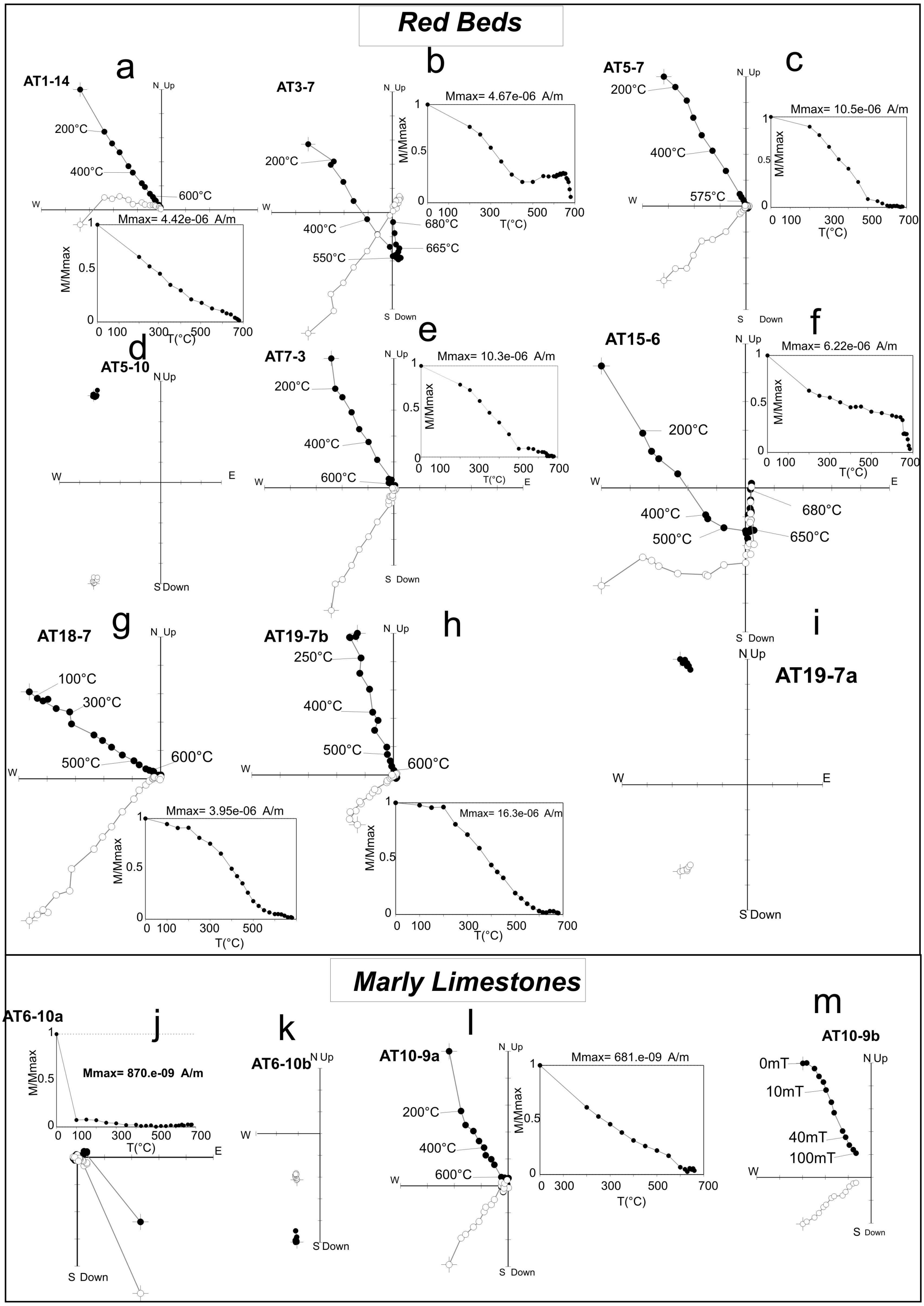

Red Beds
a
AT1-14
200°C
400°C
600°C
Mmax= 4.42e-06 A/m
b
AT3-7
Mmax= 4.67e-06 A/m
200°C
400°C
550°C
680°C
665°C
c
AT5-7
200°C
400°C
575°C
Mmax= 10.5e-06 A/m
d
AT5-10
e
AT7-3
200°C
400°C
600°C
Mmax= 10.3e-06 A/m
f
AT15-6
200°C
400°C
500°C
680°C
650°C
Mmax= 6.22e-06 A/m
g
AT18-7
100°C
300°C
500°C
600°C
Mmax= 3.95e-06 A/m
h
AT19-7b
250°C
400°C
500°C
600°C
Mmax= 16.3e-06 A/m
i
AT19-7a
M/Mmax
T(°C)
N Up
S Down
W
E
Marly Limestones
j
AT6-10a
Mmax= 870.e-09 A/m
k
AT6-10b
l
AT10-9a
200°C
400°C
600°C
Mmax= 681.e-09 A/m
m
AT10-9b
0mT
10mT
40mT
100mT

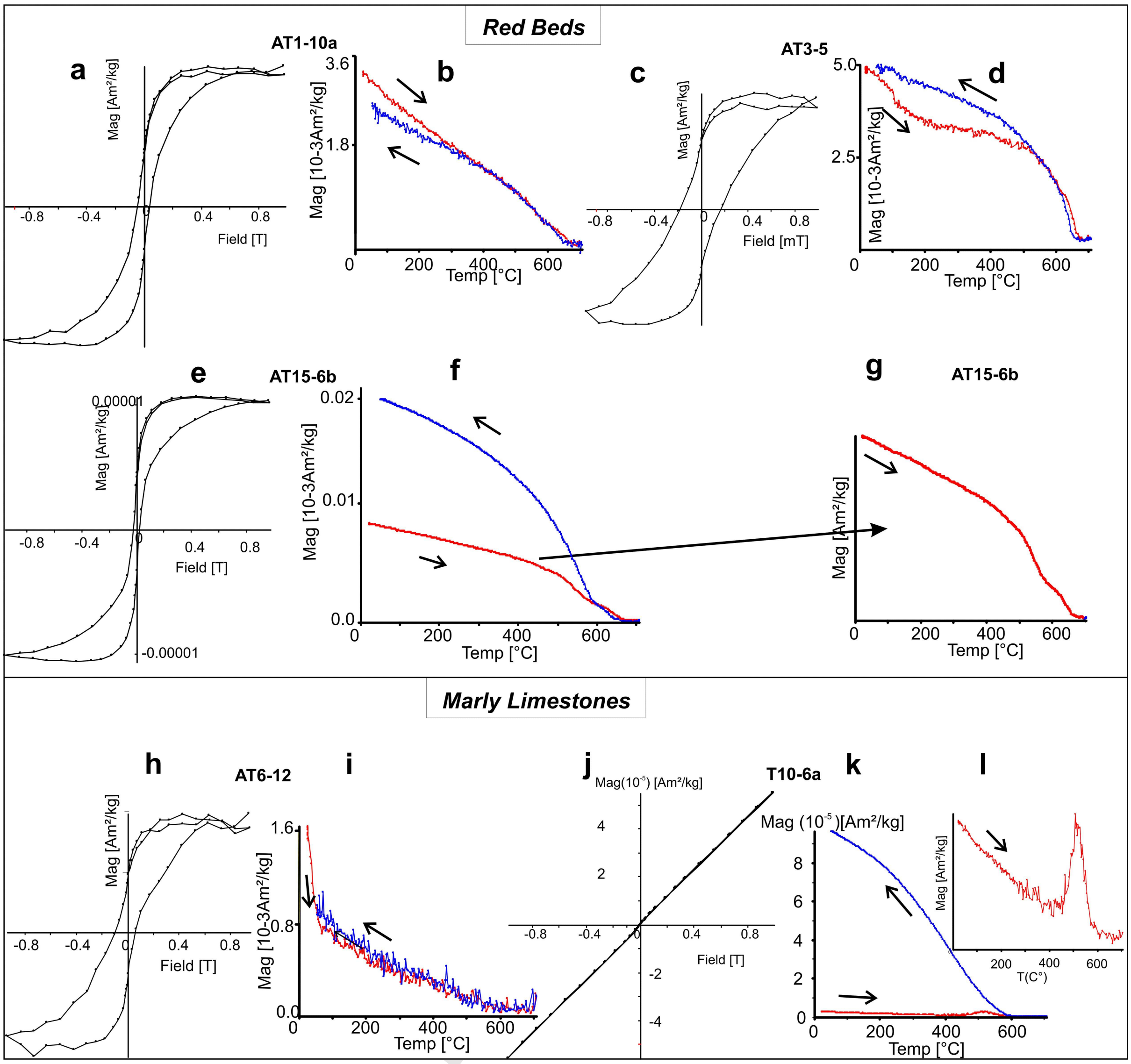

Red Beds
AT1-10a
a
Mag [Am²/kg]
Field [T]
b
Mag [10-3Am²/kg]
Temp [°C]
c
AT3-5
Mag [Am²/kg]
Field [mT]
d
Mag [10-3Am²/kg]
Temp [°C]
e
AT15-6b
Mag [Am²/kg]
Field [T]
f
Mag [10-3Am²/kg]
Temp [°C]
g
AT15-6b
Mag [Am²/kg]
Temp [°C]
Marly Limestones
h
AT6-12
Mag [Am²/kg]
Field [T]
i
Mag [10-3Am²/kg]
Temp [°C]
j
Mag(10⁻⁵) [Am²/kg]
Field [T]
T10-6a
k
Mag (10⁻⁵)[Am²/kg]
Temp [°C]
l
Mag [Am²/kg]
T(C°)

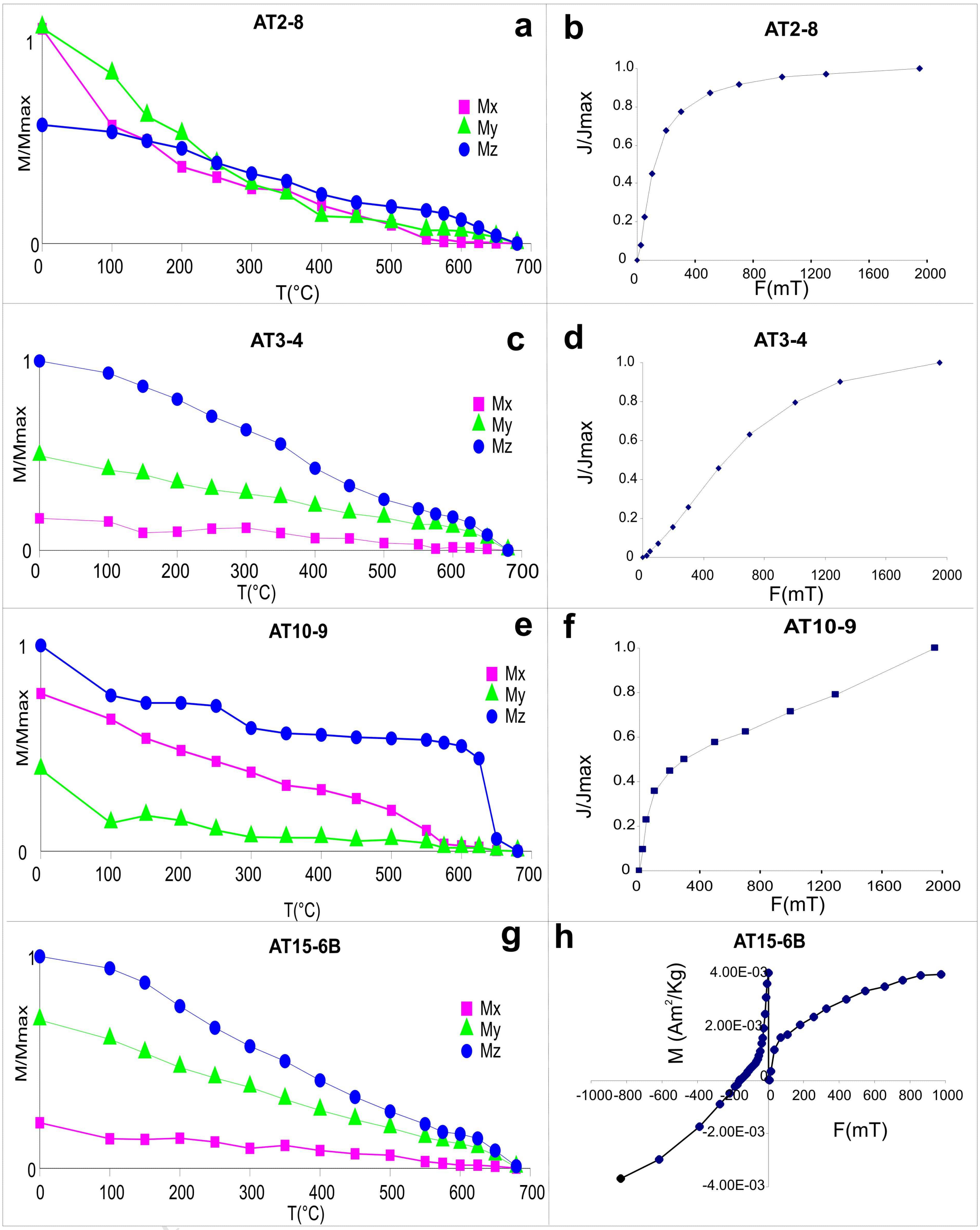

a
AT2-8
M/Mmax
Mx
My
Mz
T(°C)
b
AT2-8
J/Jmax
F(mT)
c
AT3-4
M/Mmax
Mx
My
Mz
T(°C)
d
AT3-4
J/Jmax
F(mT)
e
AT10-9
M/Mmax
Mx
My
Mz
T(°C)
f
AT10-9
J/Jmax
F(mT)
g
AT15-6B
M/Mmax
Mx
My
Mz
T(°C)
h
AT15-6B
M (Am²/Kg)
4.00E-03
2.00E-03
-2.00E-03
-4.00E-03
F(mT)

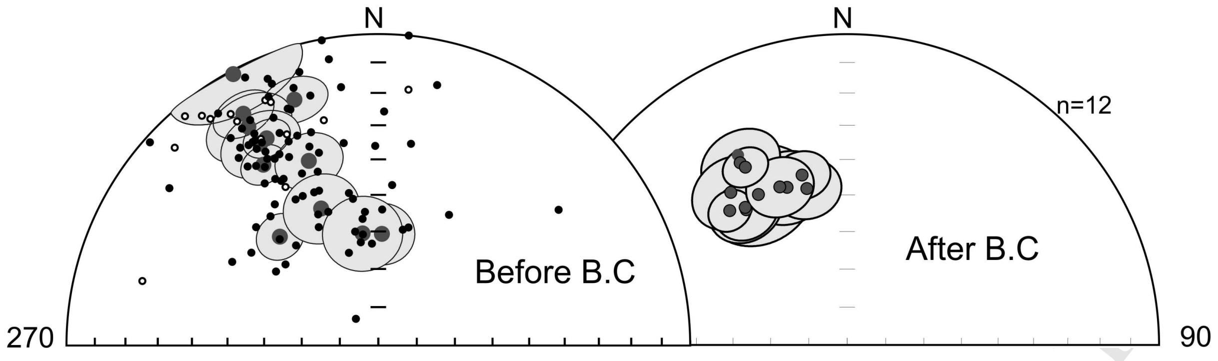
N
Before B.C
270
N
n=12
After B.C
90

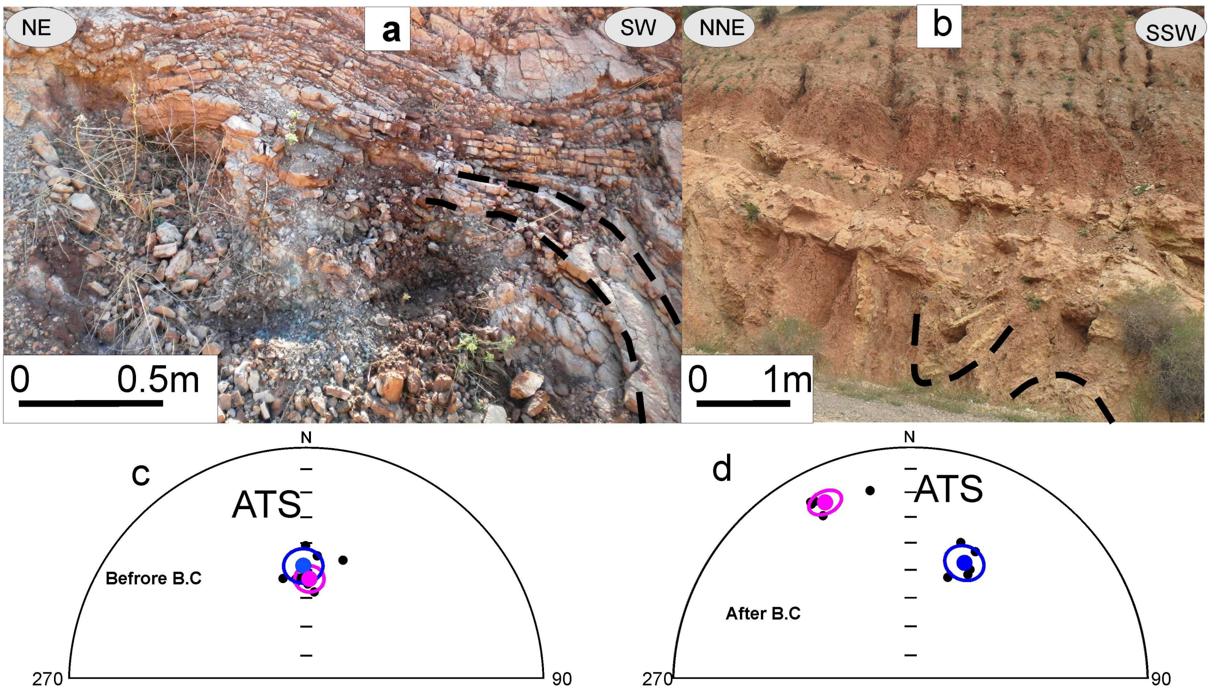
NE
a
SW
0 0.5m
NNE
b
SSW
0 1m
N
c
ATS
Befrore B.C
270
90
N
d
ATS
After B.C
270
90

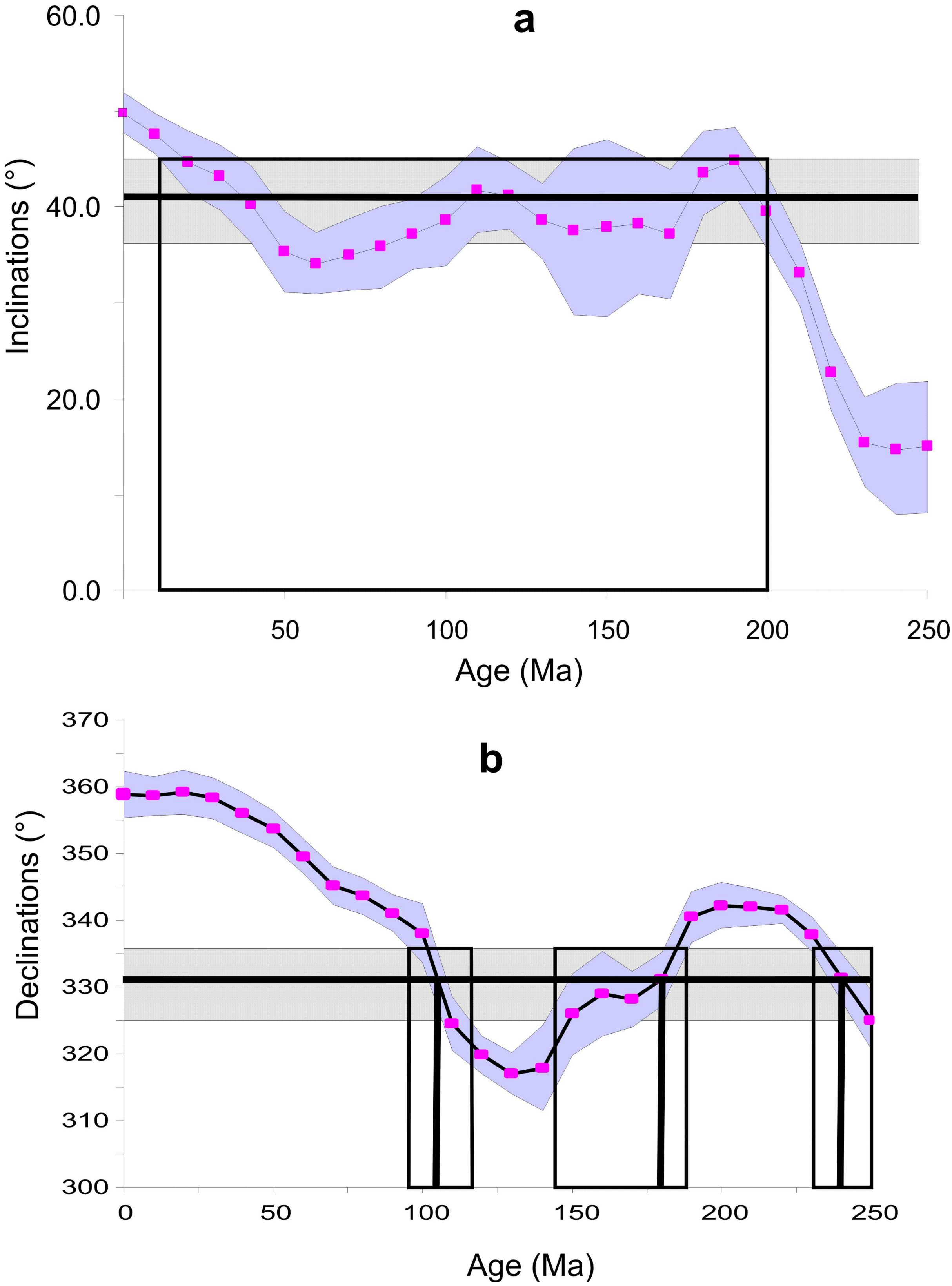
a
60.0
40.0
20.0
0.0
Inclinations (°)
50
100
150
200
250
Age (Ma)
b
370
360
350
340
330
320
310
300
Declinations (°)
0
50
100
150
200
250
Age (Ma)

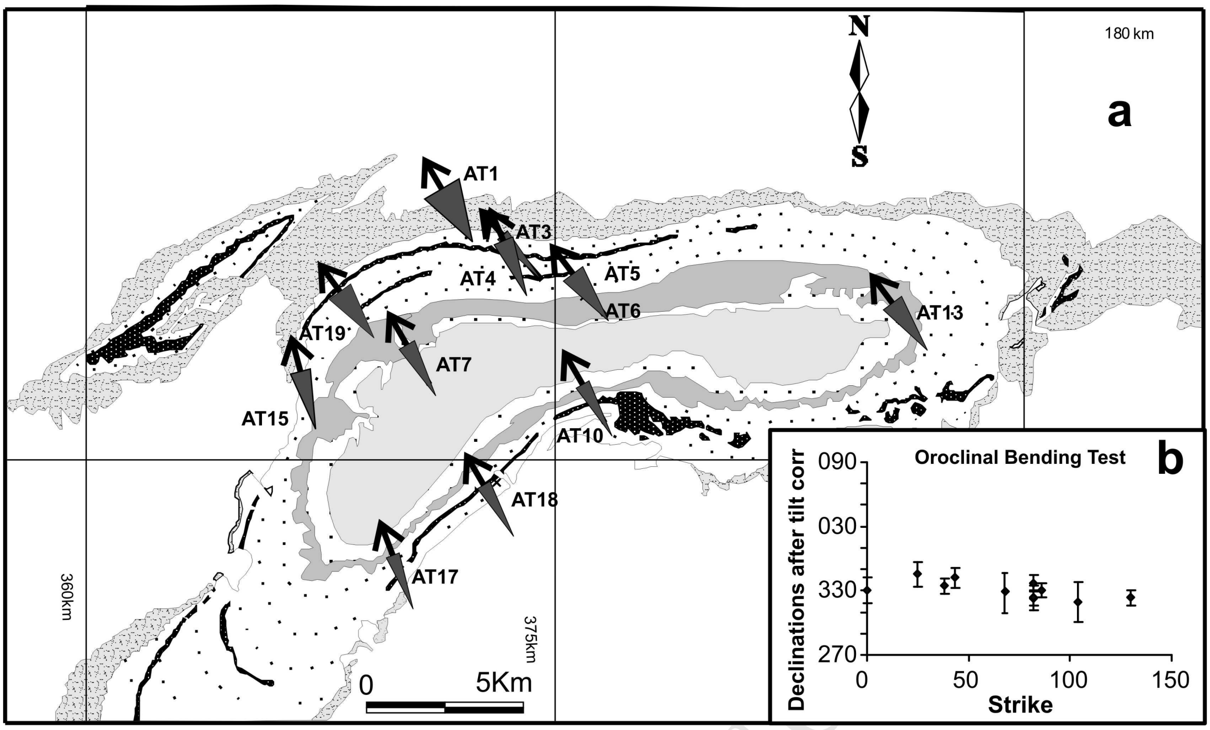
180 km
a
N
S
AT1
AT3
AT4
AT5
AT6
AT13
AT19
AT7
AT15
AT10
AT18
AT17
360km
375km
0
5Km
b
Oroclinal Bending Test
Declinations after tilt corr
090
030
330
270
0
50
100
150
Strike

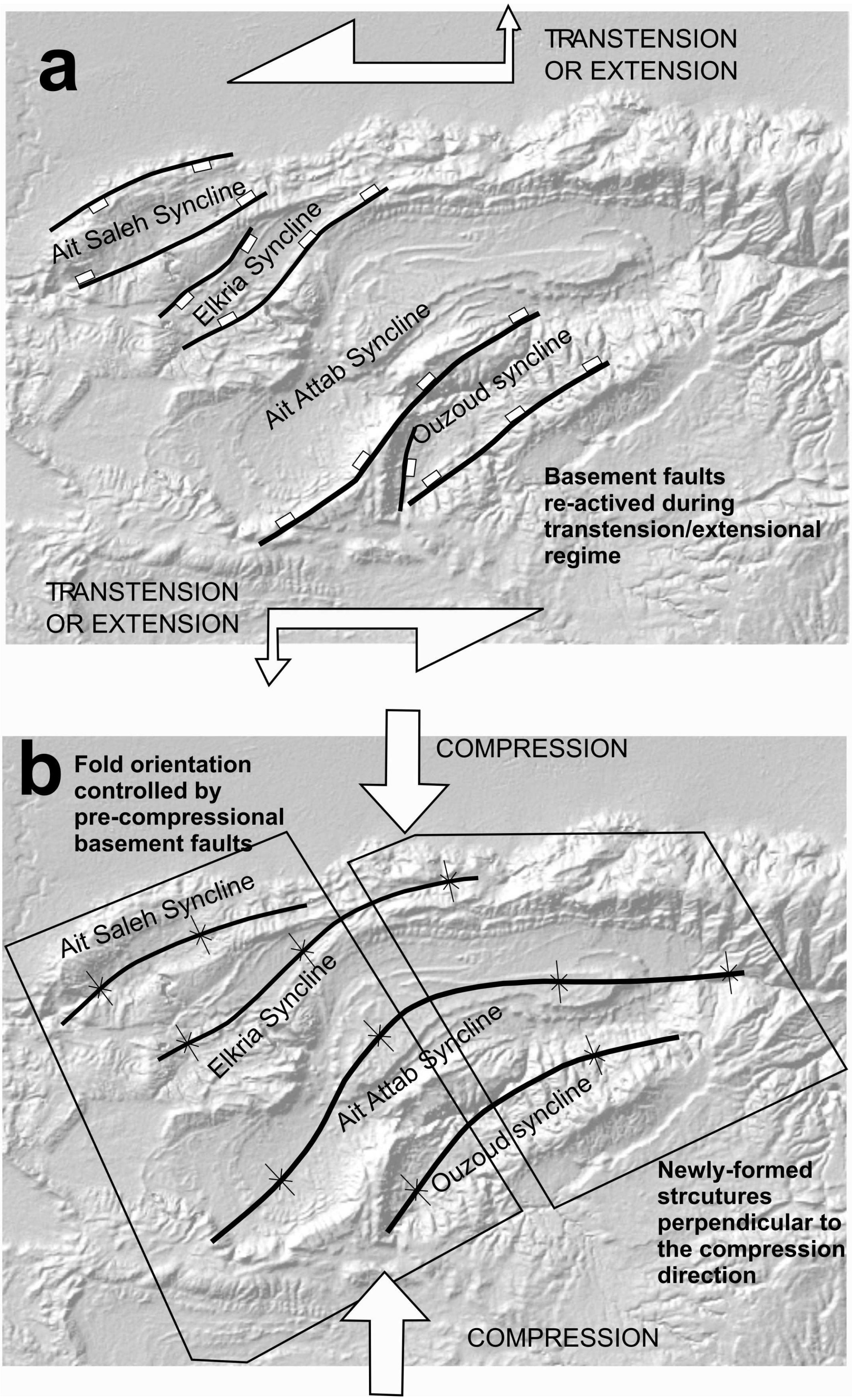
a
TRANSTENSION
OR EXTENSION
Ait Saleh Syncline
Elkria Syncline
Ait Attab Syncline
Ouzoud syncline
Basement faults
re-actived during
transtension/extensional
regime
TRANSTENSION
OR EXTENSION
COMPRESSION
b
Fold orientation
controlled by
pre-compressional
basement faults
Ait Saleh Syncline
Elkria Syncline
Ait Attab Syncline
Ouzoud syncline
Newly-formed
strcutures
perpendicular to
the compression
direction
COMPRESSION

Application of paleomagnetism to investigate basin evolution

NRM of Jurassic-Cretaceous red beds is dominated by a Cretaceous remagnetization

The remagnetization dated at 100 Ma pre-dates major folding in this area

Two stages of folding are revealed from paleomagnetism and structural analysis

Oroclinal bending vs. primary curvature of regional syncline is discriminated